Supplementary Information

Synthesis of Aligned Symmetrical Multifaceted Monolayer Hexagonal Boron Nitride Single Crystals on Resolidified Copper

Roland Yingjie Tay,[a,b] Hyo Ju Park,[c] Gyeong Hee Ryu,[c] Dunlin Tan,[a,d] Siu Hon Tsang,[b] Hongling Li,[a,d] Wenwen Liu,[a] Edwin Hang Tong Teo,[*a,e] Zonghoon Lee,[c,f] Yeshayahu Lifshitz,[g] and Rodney S. Ruoff[f,h]

[a] School of Electrical and Electronic Engineering, Nanyang Technological University, 50 Nanyang Avenue, Singapore 639798, Singapore

[b] Temasek Laboratories@NTU, 50 Nanyang Avenue, Singapore 639798, Singapore

[c] School of Materials Science and Engineering, Ulsan National Institute of Science and Technology (UNIST), Ulsan 689-798, Republic of Korea

[d] CNRS-International NTU Thales Research Alliance CINTRA UMI 3288, Research Techno Plaza, 50 Nanyang Drive, Singapore 637553, Singapore

[e] School of Materials Science and Engineering, Nanyang Technological University, 50 Nanyang Avenue, Singapore 639798, Singapore

[f] Center for Multidimensional Carbon Materials, Institute for Basic Science (IBS), Ulsan 689-798, Republic of Korea

[g] Department of Materials Science and Engineering, Technion, Israel Institute of Technology, Haifa 3200003, Israel

[h] Department of Chemistry, Ulsan National Institute of Science and Technology (UNIST), Ulsan 689-798, Republic of Korea

* *Corresponding author*. Tel: +65 67906371. E-mail address: HTTEO@ntu.edu.sg

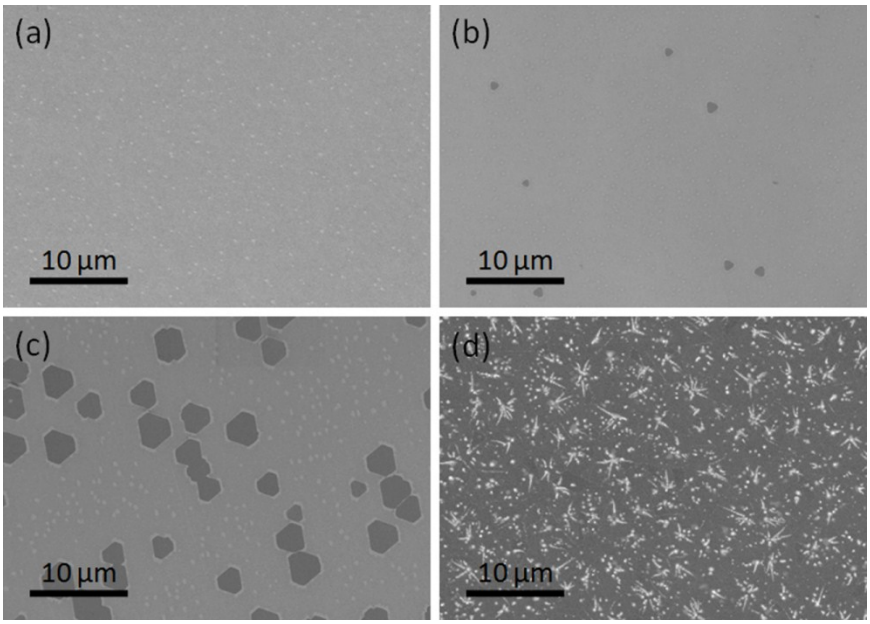

Fig. S1. Effects of h-BN nucleation on varying sublimation temperature of ammonia borane. SEM images of as-grown h-BN domains on resolidified Cu after 10 min using 8 mg of ammonia borane heated at (a) 70 °C, (b) 80 °C, (c) 85 °C and 90 °C. Both nucleation and domain size of h-BN increase with higher sublimation temperature of ammonia borane.

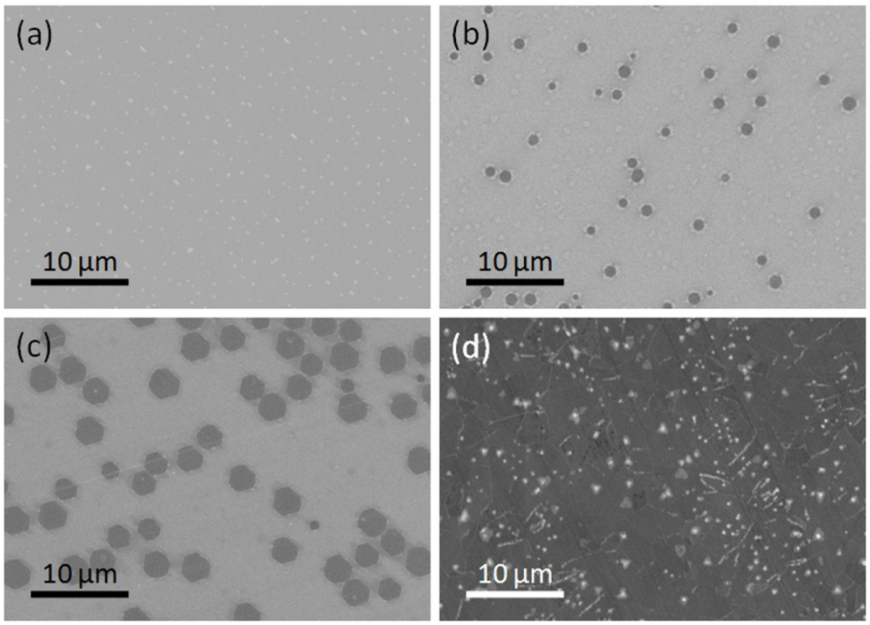

Fig. S2. Effects of h-BN nucleation on varying amount of ammonia borane. SEM images of as-grown h-BN domains on resolidified Cu after 10 min using (a) 3 mg, (b) 5 mg, (c) 8 mg and (d) 10 mg of ammonia borane heated 85 °C. Both nucleation and domain size of h-BN increase with increase amount of ammonia borane.

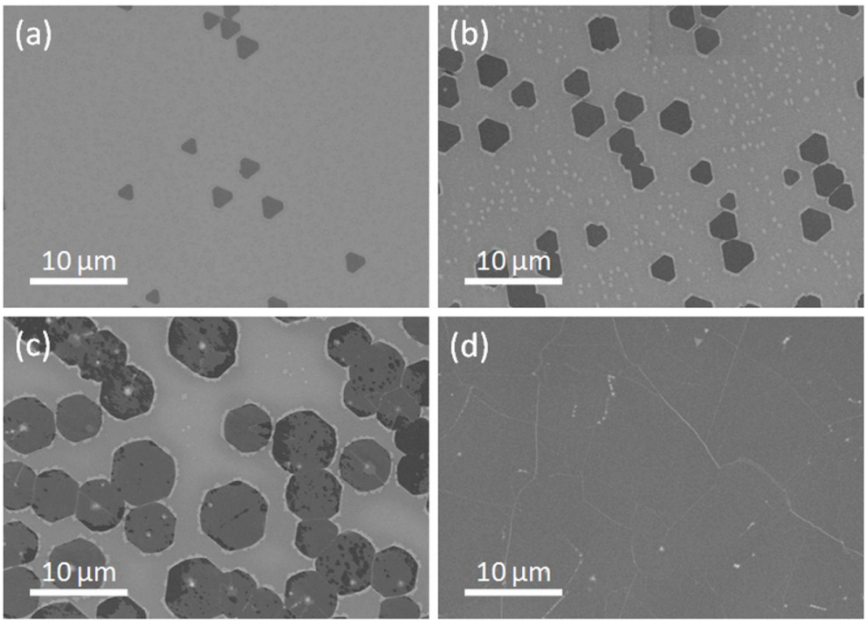

Fig. S3. Time-dependent evolution of h-BN film. SEM images of as-grown h-BN on resolidified Cu from isolated single-crystal domains to a continuous film by increasing the growth time through exposure to 8 mg of ammonia borane at a sublimation temperature of 85 °C for (a) 5 min, (b) 10 min, (c) 20 min and (d) 30 min, respectively.

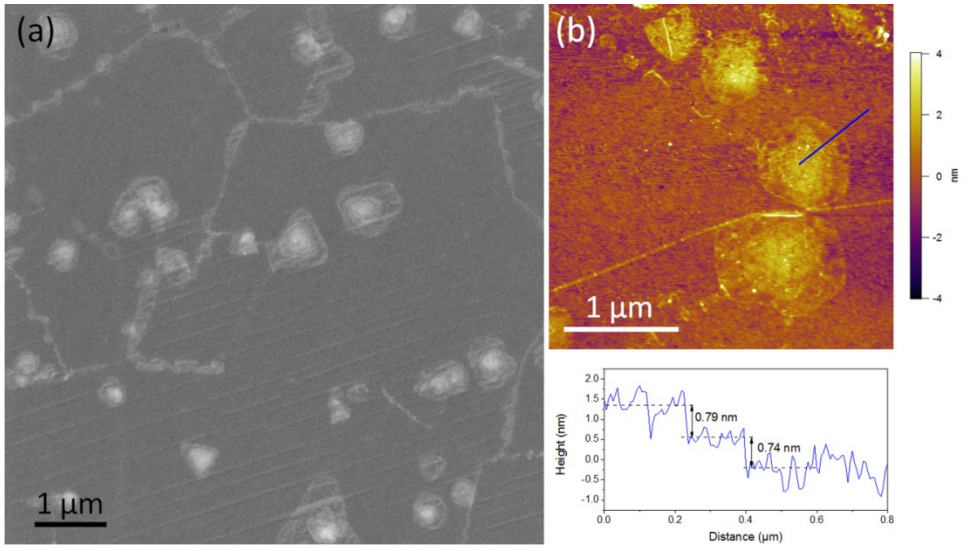

Fig. S4. Few-layer h-BN islands. (a) SEM image of a fully covered h-BN film with many few-layer islands on resolidified Cu. (b) AFM image of the transferred h-BN film in (a) onto SiO_2/Si substrate. The corresponding height profile below shows a tri-layer h-BN island.

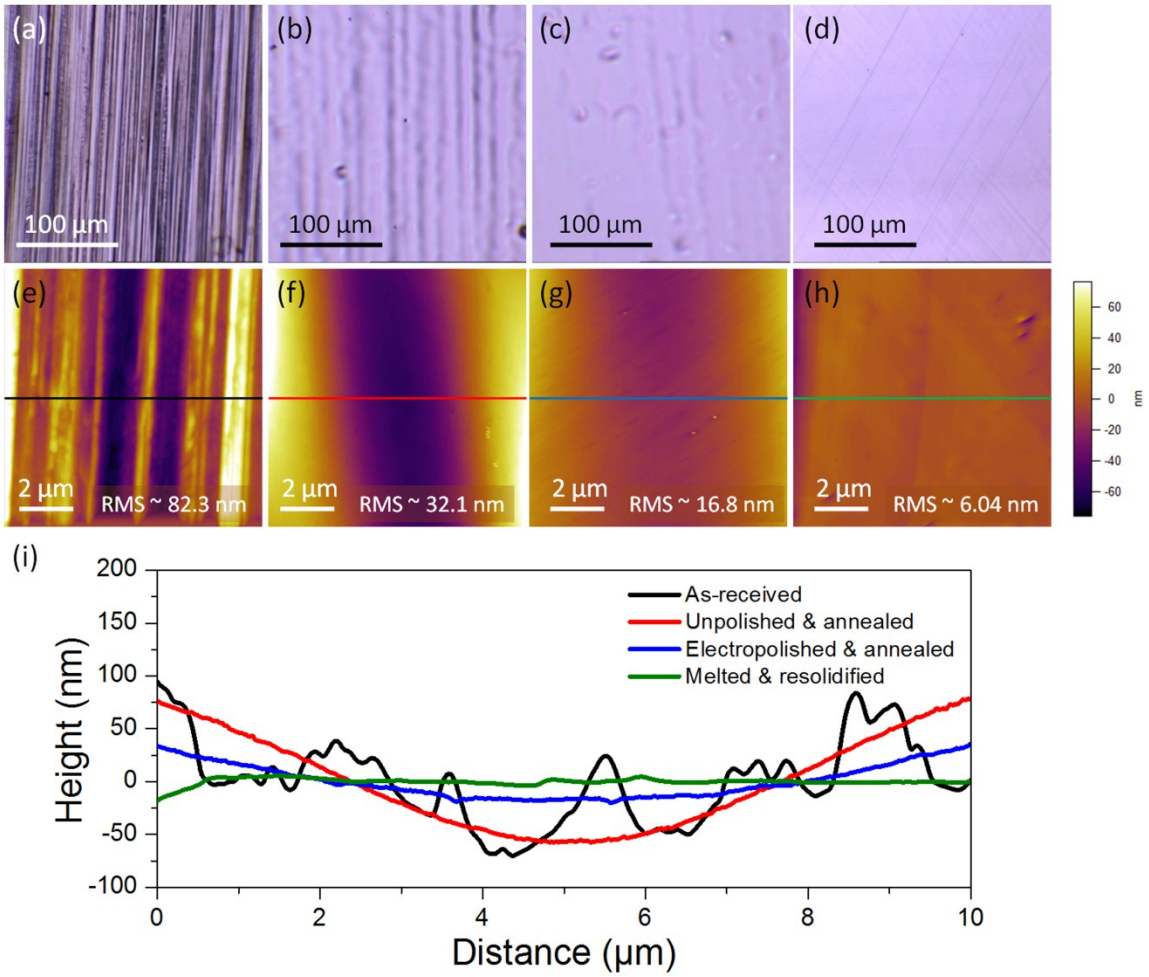

Fig. S5. Morphology comparison of various Cu substrates for h-BN growth. Representative (a–d) optical and (e–h) AFM images of as-received Cu foil, thermally annealed unpolished Cu foil, thermally annealed electropolished Cu foil and melted and resolidified Cu film to compare the difference in their surface morphologies through visual inspection and RMS roughness measurements indicated in the AFM images, respectively. (i) Plot of the height profiles on the different Cu surfaces taken from their respective AFM measurements in (e–h) are drawn in black, red, blue and green, respectively.

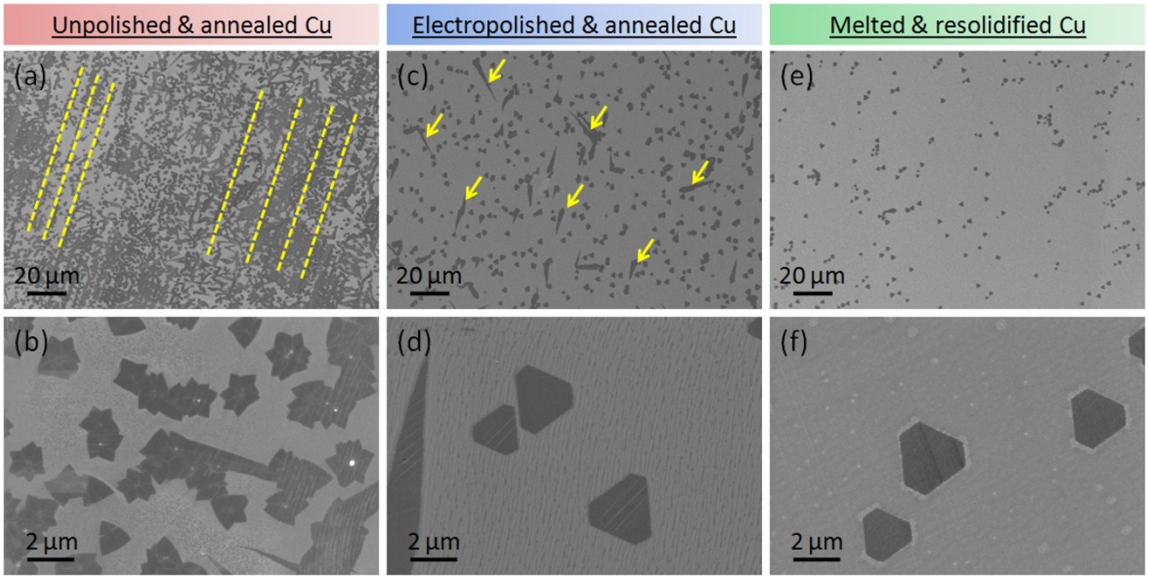

Fig. S6. Growth of h-BN single-crystal domains on Cu with different surface morphologies. The growth of h-BN single-crystal domains were done at 1050 °C for 10 min under the same exposure of 8 mg of ammonia borane at a sublimation temperature of 85 °C. SEM and magnified SEM images of as-grown h-BN single-crystal domains on (a,b) thermally annealed unpolished Cu, (c,d) thermally annealed electropolished Cu and (e,f) melted and resolidified Cu. For unpolished Cu, there is a high amount of nucleation parallel to the rolling features of the Cu (yellow dotted lines). The single-crystal domains are mostly irregular or triangular in shape and are randomly oriented. Asymmetric hexagonal domains with some irregular shapes as indicated by the yellow arrows were grown on electropolished and annealed Cu. The electropolished Cu are, however, polycrystalline and the orientation of the h-BN domains are not aligned.[1] Melted and resolidified Cu yielded the least nucleation with domains of regular shapes. The domains are well oriented following the underlying Cu(110) lattice.

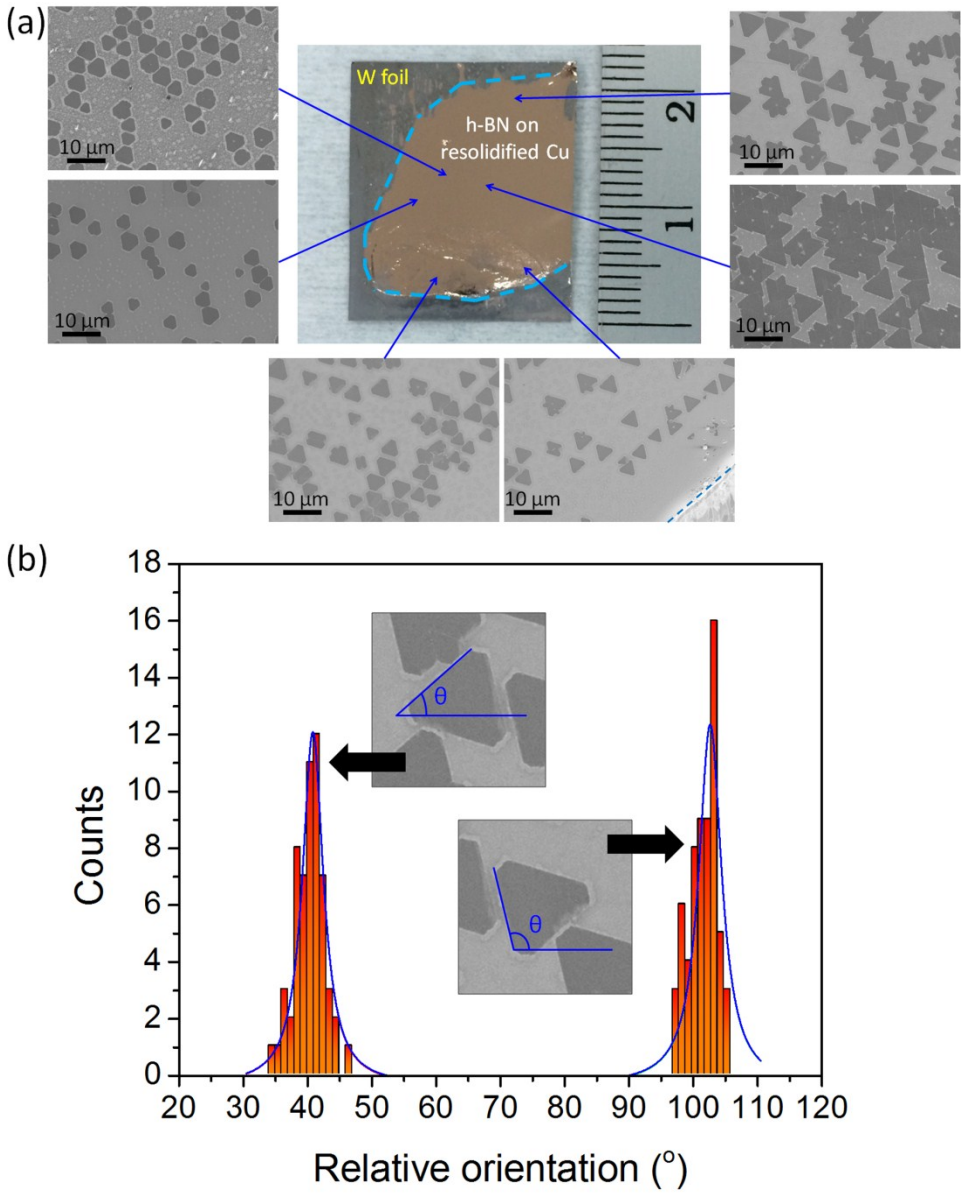

Fig. S7. Large area sampling of h-BN domains orientations on resolidified Cu surface. (a) Photograph of as-grown h-BN on resolidified Cu and SEM images taken at different regions on the Cu substrate exceeding 1 cm apart, as indicated by the blue arrows. The cyan dotted line in the photograph indicates the edge boundary between the Cu and W substrate. It is observed that the triangular and hexagonal shaped domains are distributed unevenly throughout the Cu surface. (b) Histogram plot of frequency counts against the relative orientation of the h-BN domains. The blue curve is a fitted Lorentzian distribution with two peaks centred at 40.8° and 102.3°, respectively. The insets show the extraction of the relative orientation of the h-BN domains from the SEM images. The relative orientation of the h-BN domains were extracted by measuring the angle between a straight line following the edge of the domain and a parallel line with respect to the SEM image.

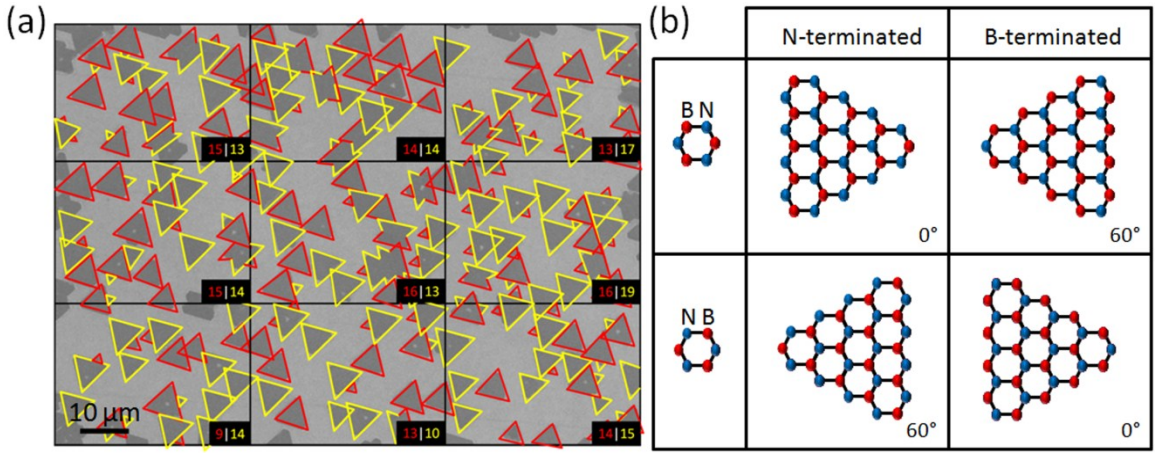

Fig. S8. Mirroring h-BN domains. (a) SEM image of as-grown triangular shaped h-BN domains on resolidified Cu. The red and yellow triangular outlines indicate the 60° rotational difference of the h-BN domains. (b) Schematic of h-BN triangular domains with different rotational orientations. From the schematic, the 60° difference can be either due to different polarity or different edge terminations. However, as N-terminated edges are favoured over B-terminated edges,[2] the 60° rotation is deduced to be caused by the two different polarities with both triangles having N-terminated edges. The ratio of red and yellow triangle count is 125:129 (1:1.03), indicating there is no favoured polarity of h-BN on Cu(110).

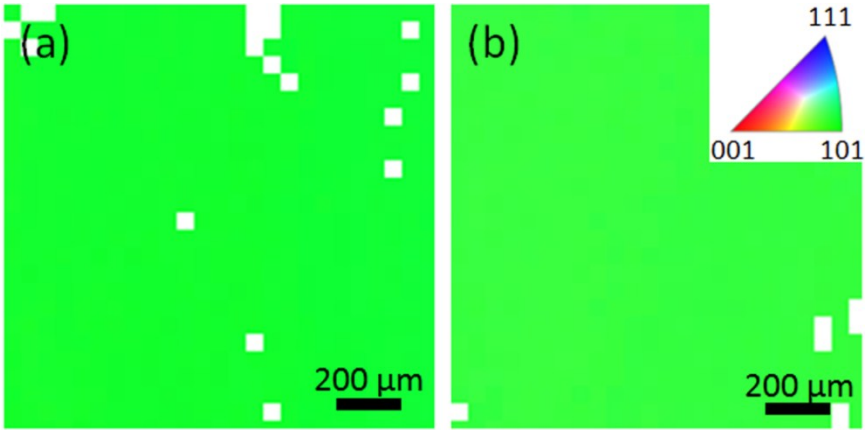

Fig. S9. Large area surface orientation mappings of resolidified Cu. (a,b) SEM/EBSD maps of the resolidified Cu taken on the same sample at over 1 cm apart. Inset of (b) shows the colour codex of the Cu lattice direction. The single green region in both the EBSD maps indicate a single crystalline Cu with (101) surface orientation for over many millimetres.

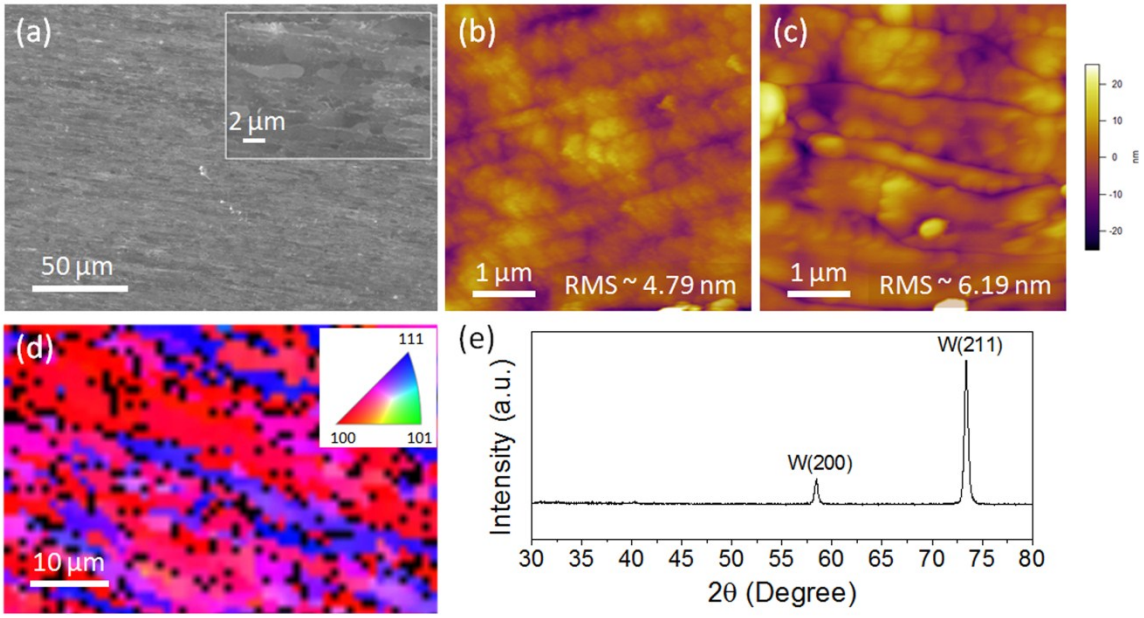

Fig. S10. Characterization of the W foil. (a) SEM image of an annealed W foil. Inset shows the corresponding magnified SEM image. AFM images of (b) as-received and (c) annealed W foil. (d) EBSD mapping of an annealed W foil. The inset shows the colour codex of the W lattice direction. (e) XRD spectrum of an annealed W foil with two peaks corresponding to the (200) and (211) surface orientations. The morphology of the polycrystalline W foil is observed to have insignificant change before and after annealing at 1090 °C. It has small grain sizes of up to a few micrometers comprising of (100) and (111) surface orientations.

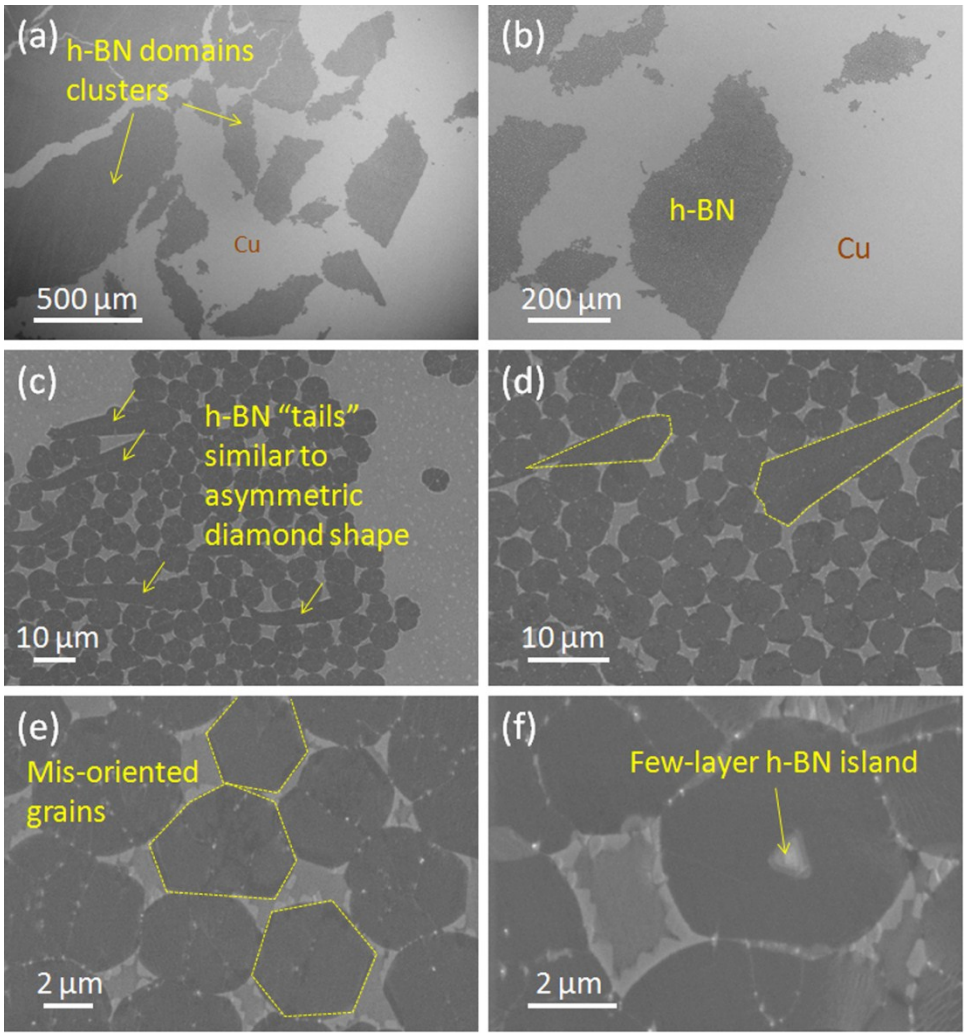

Fig. S11. Growth of h-BN on liquid Cu. (a,b) SEM images of clusters of h-BN islands grown on liquid Cu for 10 min. (c–f) Magnified SEM images within a cluster of h-BN islands in (a). Clusters of h-BN islands were observed on the Cu surface with small gaps between adjacent islands. This clustering effect has also been observed for graphene.[3] Many h-BN islands with "tails" are observed in Fig. S11c,d, similar to the asymmetric diamond structures.[4] Fig. S11e shows that the h-BN cluster consists of mis-oriented h-BN grains with lateral sizes not exceeding 10 µm. Several few-layer islands can be found on some h-BN islands in Fig. S11f.

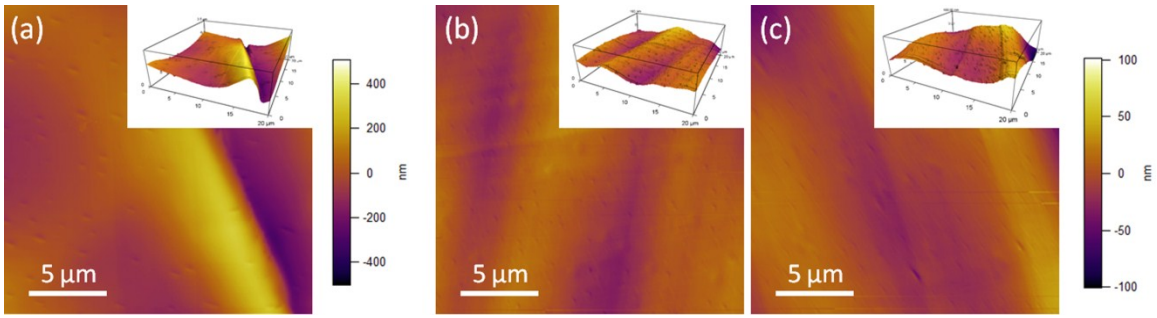

Fig. S12. Surface morphologies of resolidified Cu at different cooling rates. AFM images of resolidified Cu at the uneven regions after being (a) immediately cooled from 1090 °C and (b,c) cooled to 1075 °C at a cooling rate of 1 °C/min. The insets show their corresponding 3D AFM images.

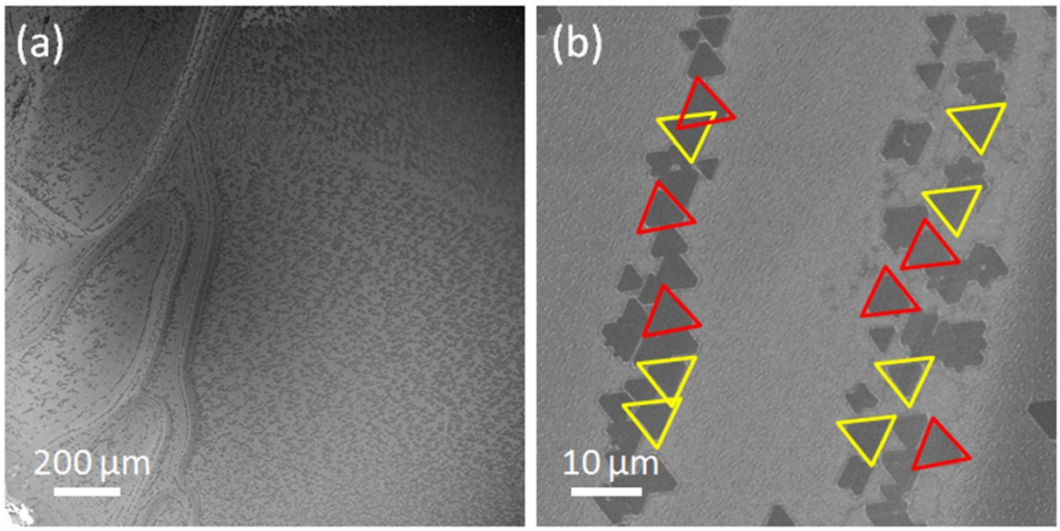

Fig. S13. Effect of uneven Cu surface on h-BN growth. (a) SEM image of as-grown h-BN domains on the uneven surface of the resolidified Cu. The resolidification cooling rate used was 1 °C/min and the growth of h-BN was carried out for 10 min under exposure to 8 mg of ammonia borane and heated at 85 °C. (b) Magnified SEM image of (a). The red and yellow triangles outline the h-BN domains.

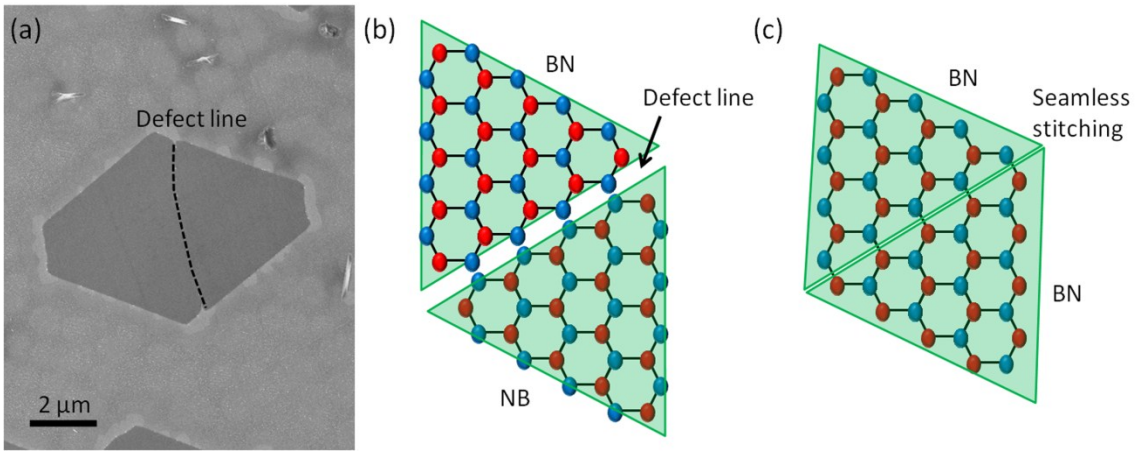

Fig. S14. Defect lines in coalescing h-BN domains. (a) SEM image of a rhombus shaped h-BN flake with a defect line between two mirroring domains. Schematic diagrams of the atomic configuration of two coalescing triangular domains with (a) different polarities and (b) same polarity. Blue and red spheres visualise N and B atoms, respectively. Due to the binary configuration of h-BN, it has two different polarities as denotes as (BN and NB) where a unit h-BN cell is rotated 60° (Fig. S14b). Fig. S14b shows the formation of a defect line caused by two N-terminated edges "meeting" each other. The N atoms cannot attach perfectly resulting in a defect line. For seamless stitching to occur, the domains must have the same polarity (Fig. S14c).

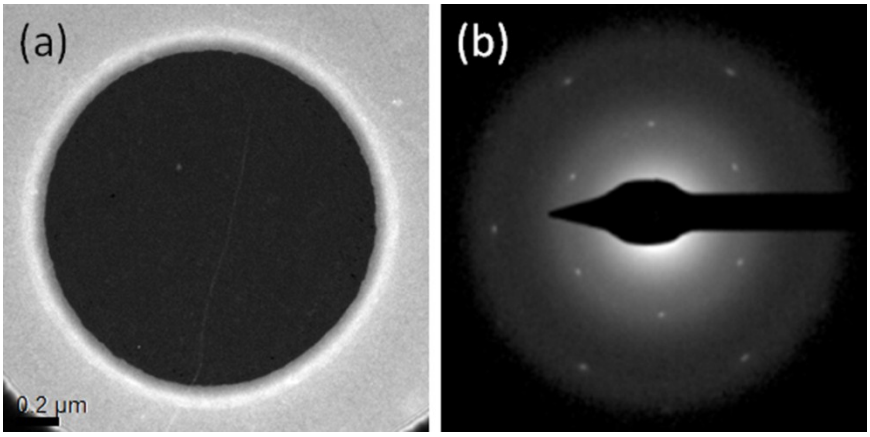

Fig. S15. Observation of a defect line. (a) DF-TEM image and its (b) corresponding SAED of two merged h-BN grains suspended above a TEM grid hole with a defect line in the middle. The two grains have an identical orientation as determined by the no change in colour contrast in the DF-TEM mapping and SAED shows only one set of hexagonal diffraction pattern.

Table S1. Relative angle measurements of h-BN single-crystal domains.

Hole no.	Relative angle (°)	Mis-orientation relative to average dominant orientation (°)
1	78.366	-1.91
2	69.193	-11.08
3	80.451	0.18
4	81.724	1.45
5	80.218	-0.05
6	53.489	-26.78
7	79.192	-1.08
8	47.974	-32.30
9	82.333	2.06
10	80.159	-0.11
11	79.526	-0.75
12	79.695	-0.58
13	80.538	0.27
14	79.584	-0.69

For SAED measurements on single-crystal h-BN domains, out of a total of 14 SAED patterns, 11 showed a similar orientation and 3 were mis-oriented (78.57% with dominant orientation). The average relative angle is 80.16° and the standard deviation is 1.12°.

Table S2. Relative angle measurements of fully covered h-BN film 1.

Hole no.	Relative angle (°)	Mis-orientation relative to average dominant orientation (°)
1	92.831	-1.01
2	93.162	-0.68
3	94.304	0.46
4	93.225	-0.62
5	95.826	1.98
6	93.286	-0.56
7	93.54	-0.30
8	93.128	-0.71
9	93.576	-0.27
10	96.216	2.37
11	96.072	2.23
12	95.87	2.03
13	89.409	-4.43
14	92.688	-1.15
15	67.8	-26.04
16	67.667	-26.17
17	67.335	-26.51
18	67.9	-25.94

For SAED measurements on full coverage h-BN film 1, out of a total 18 SAED patterns, 14 showed a similar orientation and 4 were mis-oriented (77.78% with dominant orientation). The average relative angle is 93.80° and the standard deviation is 1.81°.

Table S3. Relative angle measurements of fully covered h-BN film 2.

Hole no.	Relative angle (°)	Mis-orientation relative to average dominant orientation (°)
1	85.135	3.57
2	82.907	1.34
3	79.011	-2.55
4	83.915	2.35
5	83.239	1.67
6	99.802	18.24
7	78.818	-2.75
8	83.041	1.46
9	82.2	0.63
10	79.824	-1.74
11	79.261	-2.30
12	79.868	-1.70
13	82.995	1.43
14	98.872	17.31
15	99.03	17.46
16	98.881	17.32
17	75.217	-6.35

For SAED measurements on full coverage h-BN film 2, out of a total of 17 SAED patterns, 12 showed a similar orientation and 5 were mis-oriented (70.60% with dominant orientation). The average relative angle is 81.57° and the standard deviation is 2.25°.

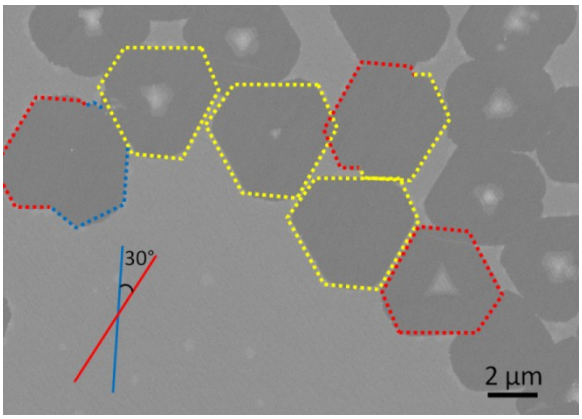

Fig. S16. SEM image of a mis-oriented h-BN domain grown on resolidified Cu. The red and yellow dotted outline the edges of the domains with 60° rotational difference (both are equivalent to the dominant orientation) and the blue dotted outline a domain with 30° mis-rotation from the dominant orientation. The inset at the bottom left shows the rotational difference of the red and blue domains.

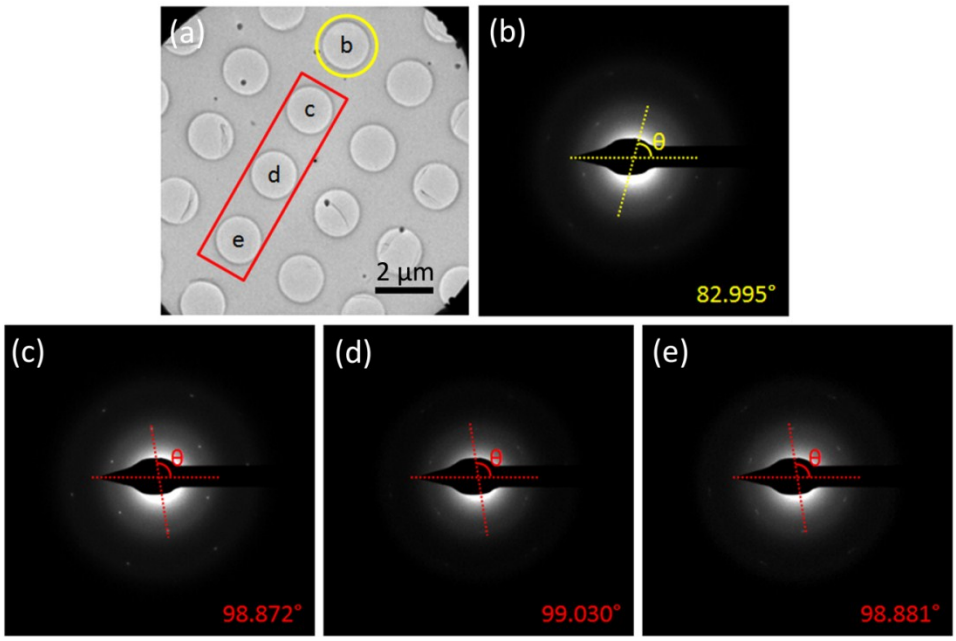

Fig. S17. Cluster of "secondary" orientation in h-BN film. (a) BF-TEM image of a transferred h-BN film on a TEM grid. (b–e) SAED patterns taken at the corresponding grid holes as labelled in (a). The relative angles of the h-BN lattice are indicated at the bottom right of the SAED images. Fig. S17b shows the dominant orientation of the h-BN film as confirmed by other SAED patterns taken at other regions of the film. Fig. S17c–e shows a cluster of the "secondary" orientation of the h-BN film taken at adjacent grid holes. These "secondary" orientations have a similar degree of mis-orientation from the dominant.

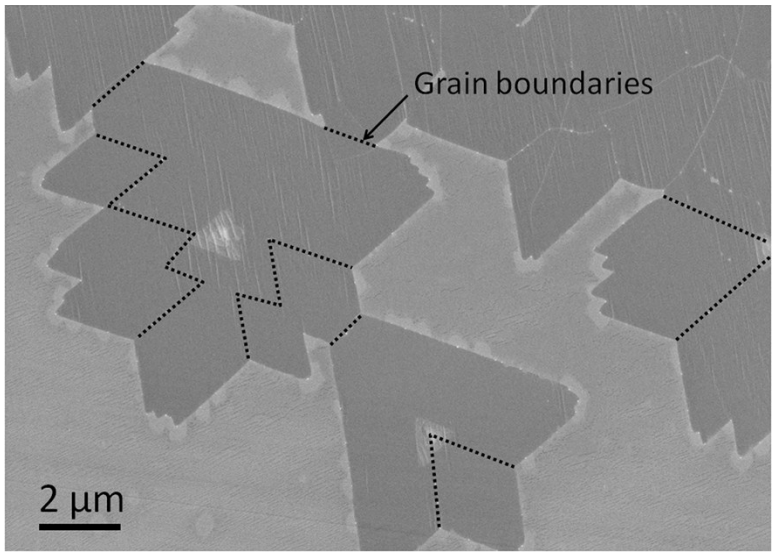

Fig. S18. Grain boundaries in merged h-BN domains. SEM image of a partially continuous film formed by merged h-BN domains. The black dotted lines indicates the grain boundaries or defect lines.

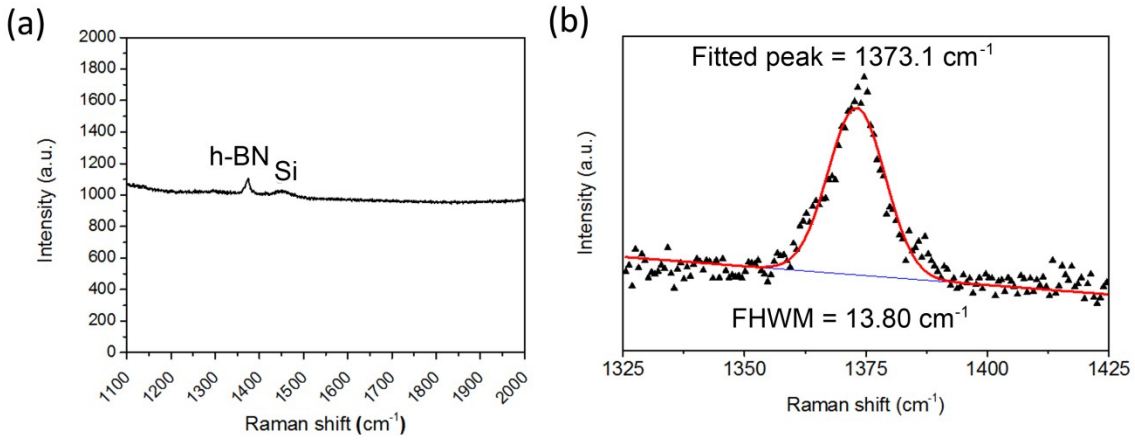

Fig. S19. Raman spectrum of h-BN film. (a) Raman spectrum of transferred h-BN film on SiO_2/Si substrate acquired using laser excitation wavelength of 532 nm (photon energy of 2.33 eV). The sharp peak at ~1370 cm^{-1} correspond to the E_{2g} vibration mode of h-BN[5] and the smaller band at ~1450 cm^{-1} is assigned to the third order Si transverse optical (TO) phonon mode.[6] (b) Fitted Raman peak and the FWHM of the h-BN monolayer film were extracted at 1373.1 cm^{-1} and 13.80 cm^{-1}, respectively.

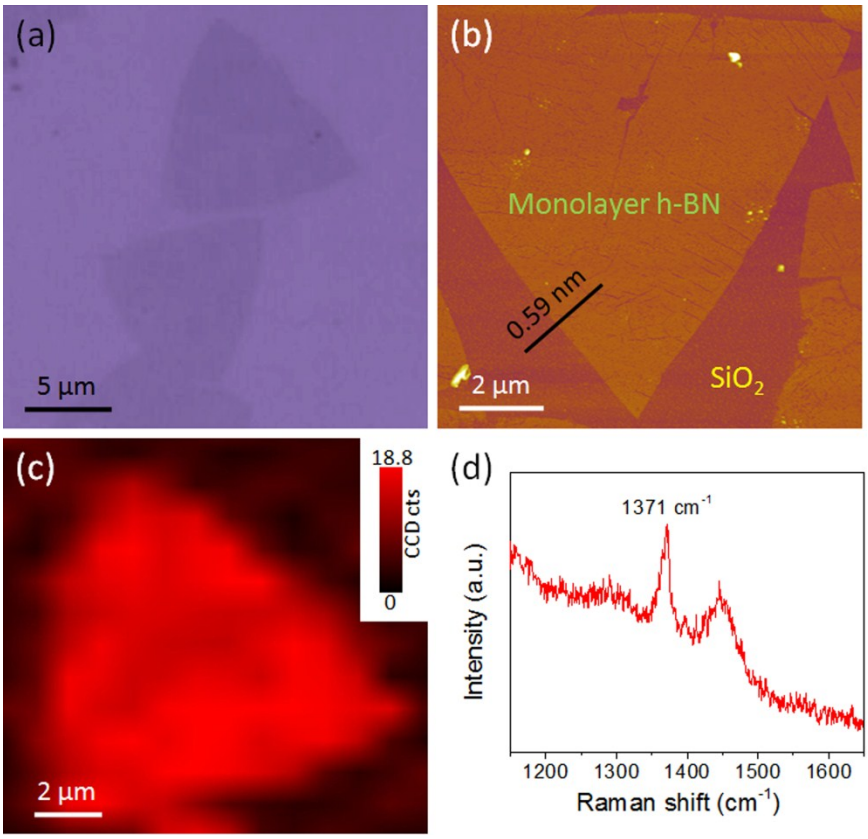

Fig. S20. AFM and Raman characterisations of monolayer h-BN single crystals. (a) Optical image of transferred h-BN single crystals on SiO_2/Si substrate. (b) AFM image and (c) Raman mapping of an isolated h-BN single-crystal domain. (d) Representative Raman spectrum of the monolayer h-BN domain.

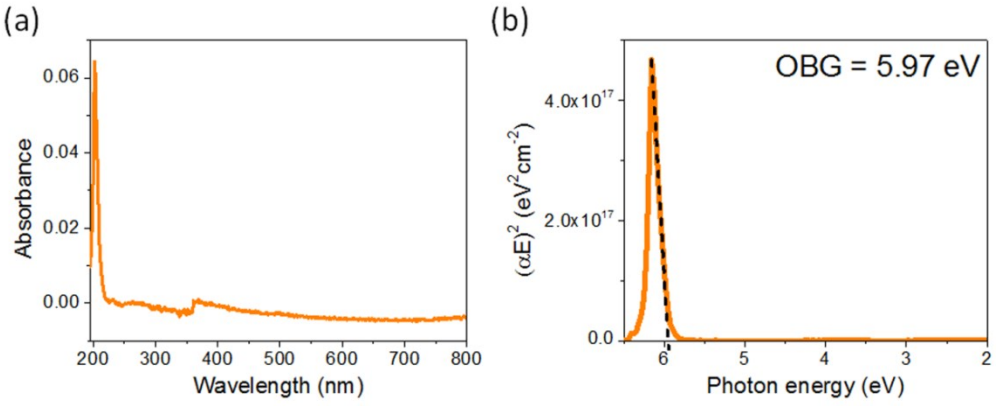

Fig. S21. OBG measurement of transferred monolayer h-BN film on quartz substrate. (a) Absorbance spectrum measured using UV-vis spectroscopy with a sharp peak at 202 nm. (b) Plot of $(\alpha E)^2$ vs. E. For a direct band gap semiconductor,[7] the absorption coefficient, $\alpha = C(E - E_g)^{1/2}/E$. C is a constant, E is the photon energy and E_g is the OBG. α is given by A/d, where A is the optical absorbance and d is the thickness of the h-BN film (0.58 nm measured by AFM). Extrapolation of the straight line part of the curve intersects the x-axis at OBG = 5.97 eV.

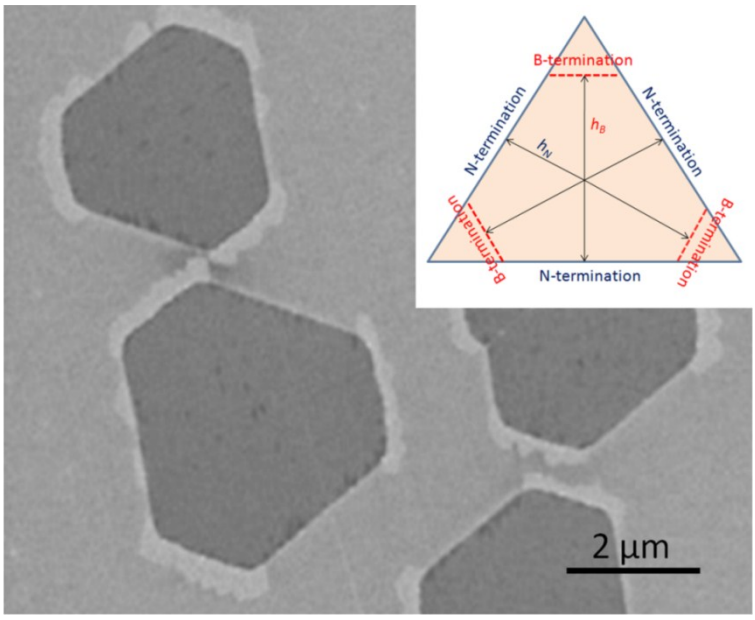

Fig. S22. Formation of asymmetric hexagonal shaped monolayer h-BN domains. SEM image of typical asymmetric hexagonal single-crystal monolayer h-BN domains grown on resolidified Cu. The inset shows the Wulff construction[8] of an asymmetric hexagonal shaped h-BN crystal. h_N and h_B denote the perpendicular distance from N- and B-zigzag edges, which are proportional to the free energy of their respective edges.

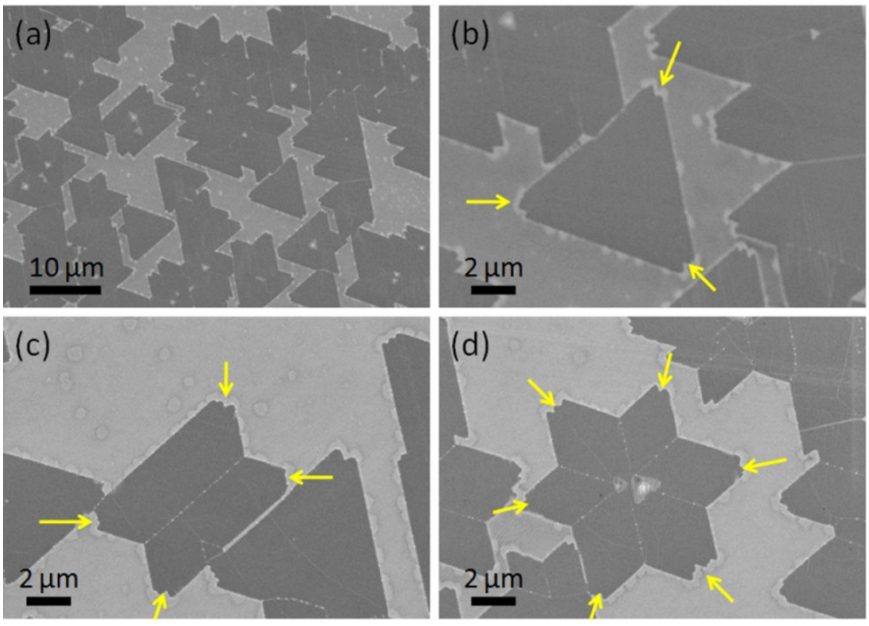

Fig. S23. Truncated edges of triangular h-BN domains. (a) SEM image taken over multiple triangular h-BN domains. Magnified SEM images of (b) a single-crystal triangular domain, (c) butterfly shaped and (d) 6-apex star shaped of merged h-BN domains. The yellow arrows indicate the truncated edges of the domains.

References

1. R. Y. Tay, M. H. Griep, G. Mallick, S. H. Tsang, R. S. Singh, T. Tumlin, E. H. T. Teo and S. P. Karna, *Nano Lett.*, 2014, **14**, 839–846.
2. Y. Liu, S. Bhowmick and B. I. Yakobson, *Nano Lett.*, 2011, **11**, 3113–3116.
3. D. Geng, B. Wu, Y. Guo, L. Huang, Y. Xue, J. Chen, G. Yu, L. Jiang, W. Hu and Y. Liu, *Proc. Natl. Acad. Sci. U.S.A.*, 2012, **109**, 7992–7996.
4. K. K. Kim, A. Hsu, X. Jia, S. M. Kim, Y. Shi, M. Hofmann, D. Nezich, J. F. Rodriguez-Nieva, M. Dresselhaus, T. Palacios and J. Kong, *Nano Lett.*, 2012, **12**, 161–166.
5. R. V. Gorbachev, I. Riaz, R. R. Nair, R. Jalil, L. Britnell, B. D. Belle, E. W. Hill, K. S. Novoselov, K. Watanabe, T. Taniguchi, A. K. Geim and P. Blake, *Small*, 2011, **7**, 465–468.
6. P. G. Spizzirri, J.-H. Fang, S. Rubanov, E. Gauja and S. Prawer, *arXiv:1002.2692v1*, 2010.
7. T. H. Yuzuriha and D. W. Hess, *Thin Solid Films*, 1986, **140**, 199–207.
8. G. Wulff and Z. Krist, *Krystallogr. Mineral.,* 1901, **34**, 449.